Journal of Non-Crystalline Solids xxx (xxxx) 122173

Contents lists available at ScienceDirect

Journal of Non-Crystalline Solids

journal homepage: www.elsevier.com/locate/jnoncrysol

Niobium incorporation into rare-earth doped aluminophosphate glasses: Structural characterization, optical properties, and luminescence

José Henrique Faleiro [a], Noelio O. Dantas [b], Anielle C.A. Silva [b], Helliomar P. Barbosa [a], Bruno H.S.T. da Silva [c], Karmel de O. Lima [d], Guilherme de Freitas Silva [d], Rogéria Rocha Gonçalves [d], Rodrigo Falci [e], Younès Messadeq [e], Isabela Dias de Oliveira Branco [f], Bianca M. Cerrutti [f], Henrik Bradtmüller [g], Hellmut Eckert [f, h], Jefferson Luis Ferrari [a, *]

[a] Desenvolvimento de Materiais Inorgânicos com Terras Raras (DeMITeR), Laboratório de Materiais Fotoluminescentes (LAMAF), Instituto de Química – (IQ), Universidade Federal de Uberlândia – (UFU), Av. João Naves de Ávila, 2121 – Bairro Santa Mônica, CEP, Uberlândia, MG 38400-902, Brazil
[b] Laboratório de Novos Materiais Nanoestruturais e Funcionais (LNMIS), Instituto de Física, Universidade Federal de Alagoas, Av. Lourival de Melo Mota, s/n, Maceió, AL 57072-900, Brazil
[c] Núcleo de Pesquisa em Síntese Orgânica e Catálise (NuPSOC) - Laboratório de Materiais Fotoluminescentes (LAMAF) - Instituto de Química da Universidade Federal de Uberlândia UFU, Av. João Naves de Ávila, 2121 – Bairro Santa Mônica, CEP, Uberlândia, MG 38400-902, Brazil
[d] Laboratório de Materiais Luminescentes Micro e Nanoestruturados –Mater Lumen, Departamento de Química, FFCLRP, Universidade de São Paulo, Av. Bandeirantes, 3900, CEP, Ribeirão Preto, SP 14040-901, Brazil
[e] Centre d'Optique et Photonique et Laser, Laval University, Quebéc, Canada
[f] São Carlos Institute of Physics, University of São Paulo, São Carlos, SP 13560-590, Brazil
[g] Department of Materials Engineering, Federal University of Sao Carlos, Sao Carlos, SP 13565-905, Brazil
[h] Institut für Physikalische Chemie, WWU Münster, Corrensstr. 30, Münster D48149, Germany

ARTICLE INFO

Keywords:
Niobium phosphate glass
Rare earth ion doping
Energy conversion
Photoluminescence
Downshifting
Glass structure
NMR spectroscopy

ABSTRACT

Luminescent Rare Earth (RE^{3+}) doped phosphate glasses with molar composition (1-x)($60P_2O_5$ – $15ZnO$ – $5Al_2O_3$ – $10BaO$ – $10PbO$)-xNb_2O_5 (x = 0, 10, 20 and 30 wt%) doped with 1.0, 1.2 and 0.3 wt% of Eu_2O_3, Yb_2O_3 and Er_2O_3, respectively, were prepared by conventional melt cooling. The glasses were characterized by optical reflectance, Raman scattering, and multinuclear (^{31}P, ^{27}Al, and ^{93}Nb) solid-state NMR spectroscopy. Monotonic ^{31}P chemical shift changes as a function of Nb_2O_5 content are consistent with the successive formation of Nb-O-P linkages. Aluminum is found in four-, five-, and six-coordination, with a successive decrease in average coordination number with increasing niobium content, while ^{93}Nb NMR indicates three distinct niobium environments in these glasses. Incorporation of Nb_2O_5 has the expected effects on refractive index values, optical basicity, optical electronegativity, Urbach Energy, and the indirect bandgap, while RE^{3+} emission properties are only slightly modified. Under UV excitation, narrow emission bands are observed arising from $^5D_0 \rightarrow {}^7F_J$ (J = 0, 1, 2, 3, and 4) transitions of Eu^{3+}. At least two distinct Eu^{3+} lifetime values are observed, suggesting a spread of different ionic environments within the glass structure. Co-doping with Er^{3+}/Yb^{3+} promotes emission in the infrared region, with a maximum of band emission near 1535 nm and a width of 30.65 nm under excitation at 980 nm. Based on the results, these glasses may be potential candidates for energy conversion from infrared or UV region to the visible region and also infrared solid-state emitters.

1. Introduction

Rare earth (RE^{3+}) ion-doped glasses are important optical and luminescent materials for photonic applications such as lasers, lighting, high-energy radiation sensing, optical thermometry, solar spectrum manipulation, bioimaging, and biosensing. The development of laser materials relies on matrices with high mechanical resistance, chemical stability, thermal diffusivity, thermal conductivity, and low phonon energy. However, certain low-phonon-energy glasses lack the mechanical and chemical resistance quality required for laser glasses and other high-power devices [1–4]. Due to properties such as wide transparency in the NUV–visible range, low phonon energies, isotropic refractive in-

* Corresponding author.
E-mail address: jeffersonferrari@ufu.br (J.L. Ferrari).

https://doi.org/10.1016/j.jnoncrysol.2023.122173
Received 29 August 2022; Received in revised form 24 January 2023; Accepted 26 January 2023
0022-3093/

dexes, and their minimal propagation losses, phosphate glasses are effective hosts for RE^{3+} ions. Furthermore, when Eu^{3+} ions occupy non-centrosymmetric locations in the host, they show strong emission in the red-orange region, around 612 nm arising from the $^5D_0 \rightarrow {}^7F_2$ transition [5], whereas co-doping with Er^{3+}/Yb^{3+} promotes emission in the infrared region, with a maximum of around 1535 nm or then the emission in the visible range assigned to the upconversion process.

The PZABP system (P_2O_5–ZnO–Al_2O_3–BaO–PbO) has been widely previously investigated, due to a favorable combination of properties such as high mechanical resistance with high thermal expansion coefficient, high refractive index, low melting trápalatemperatures, and high thermal and chemical stability. PZABP glasses also may host RE^{3+} dopants at high concentration levels, which has been attributed to the presence of the modifiers ZnO, BaO, and PbO [4,6–9].

The presence of Pb^{2+}, Zn^{2+}, and Ba^{2+} network modifiers tends to soften the glass network, while the intermediate oxide Al_2O_3 has the opposite effect. This may also result in profound structural changes in the RE^{3+} local environment, possibly resulting in more inhomogeneous ion dopant distributions and thus a reduction in cluster formation [3]. The inclusion of Nb_2O_5 into oxide glasses presents several additional benefits, mainly in optical non-linearity, vitrification, and glass stability [10]. According to Wójcik et al. [11] Nb_2O_5 solubility may be improved in glasses with high optical basicity, which quantifies the electron donor power of the glass matrix and is a useful measure for comparing different glass systems. This is especially relevant when these systems, such as the phosphate glass series, present different levels of Nb_2O_5 content [12].

The present work investigates the structural, electronic, optical, and spectroscopic properties of new glasses based on the PZABP composition (P_2O_5-ZnO-Al_2O_3-BaO-PbO) containing different concentrations of Nb_2O_5 (0, 10, 20, 30% by weight) and doped with 1.0, 1.2 and 0.3 wt% of Eu_2O_3, Yb_2O_3 and Er_2O_3, respectively. The local structures of these glasses have been characterized by Raman scattering and multinuclear (^{27}Al, ^{31}P, and ^{93}Nb) solid-state nuclear magnetic resonance. Based on an understanding observed physical properties and optical behavior we propose possible applications as energy converters from UV and IR for the visible light energy range, and also as possible optical amplifiers in the 3rd telecommunication window.

2. Experimental procedure

PZABP (60P_2O_5–15ZnO-5Al_2O_3–10BaO-10PbO) glass samples triply doped with 1.0, 1.2 and 0.3 wt% of Eu_2O_3, Yb_2O_3 and Er_2O_3, respectively, and incorporating 0, 10, 20 and 30 wt% of Nb_2O_5 (for compositions in wt.%, see Table 1) were prepared by the standard melt-cooling process, as reported by Kesavulu et al. [3]. Starting materials were P_2O_5, ZnO, Al_2O_3, BaO, and PbO (Vetec – PA – 99.98%), Nb_2O_5 (CBMM Brazil - 99.9%), and Er_2O_3, Yb_2O_3, and Eu_2O_3 (Sigma Aldrich 99.99%).

Mixtures of precursors with different amounts of Nb_2O_5 were heat treated at 150 °C for 1 h. Then, the mixtures were melted at 1350 °C for 30 min in an alumina crucible. Subsequently, the furnace temperature was lowered to 350 °C, at which the samples were heat treated for 24 h, to minimize the mechanical stress resulting from the thermal gradients during the cooling. The glasses were subsequently cooled to room temperature and polished on both sides using silicon carbide paper with different degree of grains, to acquire a flat and parallel surface for optical studies. X-ray diffractograms, recorded on a Rigaku Ultima IV diffractometer with Cu target (K_α wavelength) operating at 40 kV and 20 mA, confirmed the absence of crystalline material (see Fig. SI 1). Glass transition temperatures were measured on monolithic pieces by differential scanning calorimetry using a Netzsch DSC-204 differential scanning calorimeter, using a heating rate of 10 K/min.

Room temperature refractive indices were measured at 532.8, 632.8, and 1538 nm, using a Metricon Model 2021 refractometer based on the prism coupling technique [13]. Raman spectra were recorded operating a LabRam Horiba Jobin-Yvon spectrometer, using a diode laser at 532.8 nm as excitation source, with acquisition time of 3 s, lens with 10X for focal length and a detector with 600 gr/mm. The reflectance spectra were recorded using a SHIMADZU UV-1800 spectrophotometer with 5 nm slit width. Optical gap energy (E_g) and Urbach energy (UE) were determined from the experimental reflectance spectra.

Room temperature photoluminescence data were measured on a Horiba Scientific Fluorolog-3 (model FL3–22), equipped with a dual monochromator in face front mode (22.5°), using a 450 W Xenon lamp as an excitation light source in the visible range, with slit widths of 2 and 5 nm for the emission and excitation monochromators, respectively. The R928P Horiba photomultiplier was used for visible range detection. Luminescence decay curves were obtained using a pulsed lamp with 150 W of power, and recorded on a SPEX 1934D phosphorimeter, setting the excitation and emission monochromators to 392.5 and 612 nm, respectively, and their respective slit widths at 3 nm. The emission spectra recorded in the infrared region (1400–1700 nm) were measured using a diode laser excitation source at 980 nm with a 100 mW pump energy and a Hamamatsu H10330–75 photomultiplier as a detector. All curves were fitted as biexponential decays, and mean lifetime values were extracted from the data. Based on the emission spectra, the chromaticity diagrams were built. The upconversion spectra were obtained operating a Nanolog: Horiba Jobin-Yvon spectrophotometer using a 980 nm Collimated Diode Laser System as excitation source operated at power levels from 1.5 up to 5 W, and a Hamamatsu photomultiplier detection system ranging from 175 to 900 nm. Single resonance ^{31}P magic-angle spinning (MAS) NMR spectra were measured on an Agilent DD2 spectrometer interfaced with a 5.64 T magnet. Samples were spun at 10 kHz within 4 mm rotors. The spectra were acquired using 90° excitation pulses of 5 μs length, and a relaxation delay of 80 s. ^{27}Al MAS-NMR spectra were measured on a Bruker Avance Neo 600 MHz spectrometer (magnetic flux density 14.1 T), using pulses with small flip angles of 15° (0.55 μs length, MAS rotor frequency υ_{rf} = 60 kHz) and a relaxation delay of 1 s. ^{27}Al{^{31}P} rotational echo double resonance (REDOR) NMR measurements were also conducted at 14.1 T, on samples spinning at 20 kHz in 2.5 mm rotors in a commercial triple resonance probe. The standard Gullion-Schaefer [14] pulse sequence was used with ^{31}P inversion pulses of 6.3 μs length. Approximate second moments $M_{2(Al\text{-}P)}$, characterizing the strength of the ^{27}Al-^{31}P magnetic dipole-dipole interactions were obtained by applying a parabolic fit to the REDOR data within the range $\Delta S/S_0 \leq 0.2$, according to the expression [15]

Table 1
Glass compositions (in wt.%) and glass transition temperatures of the samples.

PZABP									$T_{g,on}$ / °C (±3 °C)	$T_{g,in}$ / °C (±3 °C)
Nb_2O_5	P_2O_5	ZnO	Al_2O_3	BaO	PbO	Er_2O_3	Yb_2O_3	Eu_2O_3		
PZABP	60.78	8.71	3.64	10.94	15.93				455	466
0	59.30	8.50	3.55	10.67	15.54	0.3	1.2	1.0	454	475
10	53.33	7.65	3.20	9.60	13.99	0.27	1.1	0.9	482	502
20	47.77	6.80	2,84	8.54	12.43	0.24	1.0	0.8	510	529
30	41.51	5.95	2.49	7.47	10.88	0.21	0.84	0.7	539	550

$$\frac{\Delta S}{S_0} = \frac{4}{3\pi^2}(NT_r)^2 f\, M_{2(\mathrm{Al}-P)} \quad (1)$$

In this expression, NT_r is the number of rotor cycles multiplied by the length of the rotor period, defining the dipolar mixing time, and f is a scaling factor (a number between zero and unity) that reflects experimental imperfections such as resonance offsets, π-pulse missets, and effects due to non-negligible pulse lengths in comparison with the duration of the rotor cycle. In the present investigation, we determined $f = 0.77$, accounting for the discrepancy between the theoretical (van-Vleck) and experimental $M_{2(\mathrm{Al\text{-}P})}$ value of the model compound $AlPO_4$. [16]

^{93}Nb MAS-NMR spectra were measured on the same spectrometer in a 1.3 mm rotor operated at a spinning speed of 60.0 kHz, using small flip-angle pulses of 0.6 μs length and a relaxation delay of 0.2 s. Chemical shifts are reported relative to 85% H_3PO_4, 1 M $Al(NO_3)_3$, and $NbCl_5$ solution using AlF_3, BPO_4, and $LiNbO_3$ as solid secondary standards. The ^{27}Al and ^{93}Nb MAS-central transition spectra were fitted according to the Czjzek model [17] implemented within the ssNake data processing and simulation program based on a wide distribution of quadrupolar coupling constants.

3. Results and discussion

Differential scanning calorimetry

Fig. 1 shows the differential scanning thermograms in the glass transition region. The main heat capacity change attributed to glass softening is observed between 460 and 524 °C, with the corresponding onset temperature increasing monotonically with increasing Nb_2O_5 content. For the base glass, this thermal event is preceded by a minor event at lower temperatures suggesting some partial compositional segregation of the glass. For the Nb_2O_5 containing glasses the DSC trace in the glass transition region is superimposed by an upward bending of the baseline suggesting an exothermic structural relaxation phenomenon upon sample heating. The extent of this baseline deviation increases with increasing Nb_2O_5 content. Furthermore, in analogy to the work by Kuczek et al. on the glass system P_2O_5–SiO_2–K_2O–MgO–CaO–Fe_2O_3 [18] the glass transition temperature increases with increasing transition metal oxide content. T_g increases with increasing Nb_2O_5 contents have been observed in other phosphate glasses [19] and in bioactive silicate glasses as well.

Raman spectroscopy

Fig. 2 shows the Raman spectra, indicating rather similar intensity profiles. Aside from a weak shoulder near 890 cm^{-1} no characteristic bands arising from the niobium oxide constituent can be identified. No evidence of crystallization was detected, since only rather broad bands are found. The Pb-O bond vibration is observed at 125 cm^{-1} [20]. The broad feature extending from 300 to 500 cm^{-1} is attributed to the bending modes involving bridging oxygen atoms associated with many Q^n species [21]. A broad band centered close to 720 cm^{-1} which might be deconvoluted into two components positioned at 665 cm^{-1} and 755 cm^{-1} (dashed lines in Fig. 2) can be attributed to the vibrations of bridging oxygen atoms, either within P-O-P or P-O-Nb linkages. If the O atoms link to Q^2 units, these bands are typically found below 700 cm^{-1}, whereas O atoms linking two Q^1 units are typically observed above 700 cm^{-1}. In the Q^n notation used here, the superscript n denotes the number of P-O-P linkages present. The present data indicate that the glasses contain both Q^2 and Q^1 units, with a distinct increase in the Q^1 fraction with increasing Nb_2O_5 contents. In addition, this region also contains vibrational stretching modes involving AlO_x units [22,23] The band at 890 cm^{-1} is attributed to the vibrational mode involving highly distorted NbO_6 octahedra [19,24], leading to successive spectral broadening as function of Nb_2O_5 concentration. Unfortunately, no information on the P-O bond-stretching vibrations involving non-bridging O^- species could be obtained, because at wavenumbers beyond 1100 cm^{-1} the corresponding scattering peaks are obscured by intense sample fluorescence, even in Nb-free samples and in samples not containing RE^{3+} ions. This interference was observed on different spectrometers using different excitation wavelengths, and its origin is presently unclear. Only in the sample PZABP, a small feature near 1180 cm^{-1} is observed, consistent with the presence of Q^2 units.

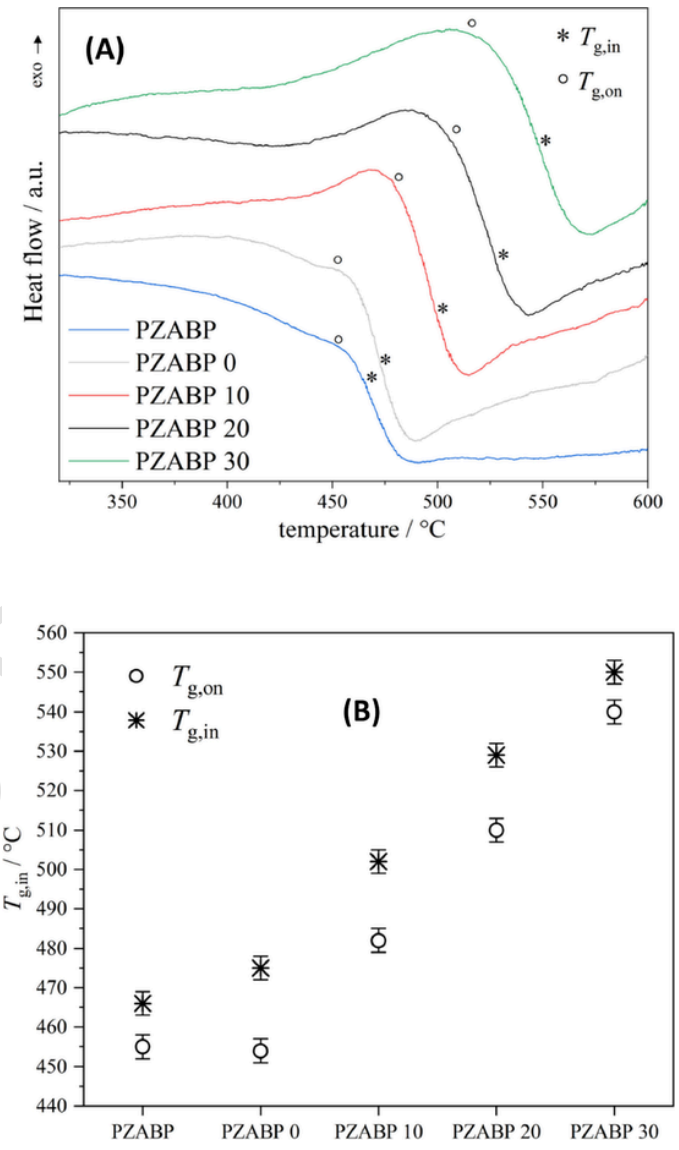

Fig. 1. (A) Differential thermograms of the samples under study. Onset and inflection points of the glass transition events are indicated by open circles and asterisks respectively. (B): Plot of onset and inflection temperatures against Nb_2O_5 content. The notations PZABP and PZABP 0 refer to rare-earth free and rare-earth doped base glasses The numerals in the other sample labels denote wt% of Nb_2O_5.

Solid-state NMR

Fig. 3 details the solid-state ^{31}P MAS NMR spectra. For the Nb-free samples, the spectra can be deconvoluted in terms of three Gaussian components centered at −11, −28, and −40 ppm (see Table 2), which can be attributed to Q^1, Q^2, and Q^3 units, respectively. The effect of RE^{3+} incorporation into the glasses is reflected in the ^{31}P spectra by a

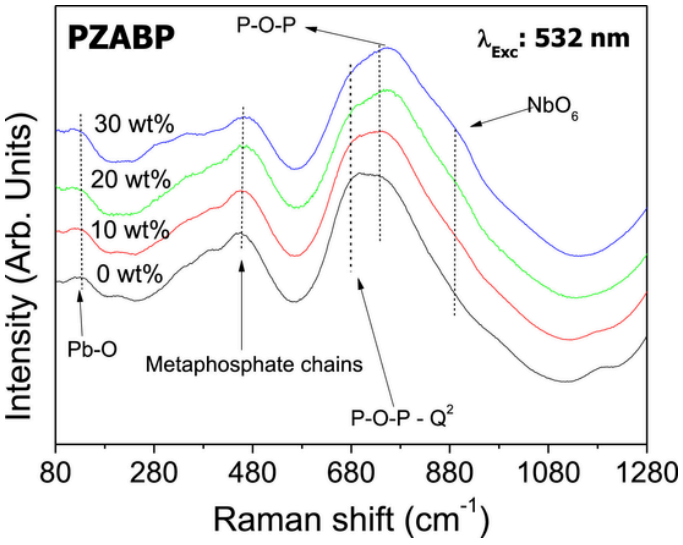

Fig. 2. Raman spectra of the PZABP glass samples doped with 1.0, 1.2 and 0.3 wt% of Eu_2O_3, Yb_2O_3 and Er_2O_3, respectively, containing Nb_2O_5 with 0.0; 10; 20 and 30 wt%.

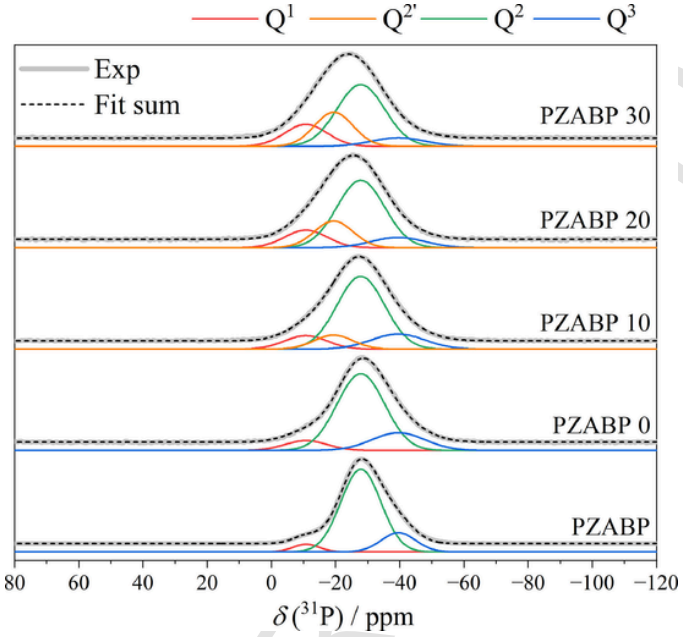

Fig. 3. ^{31}P MAS NMR spectra of the samples under study and suggested spectral deconvolutions into three or four Gaussian components (see Table 2). The notations PZABP and PZABP 0 refer to rare-earth free and rare-earth doped base glasses. The numerals in the other sample labels denote wt% of Nb_2O_5.

significant broadening of the three signal components, due to paramagnetic interactions, while their positions are otherwise invariant. For the Nb_2O_5 containing glasses the above deconvolution model does not describe the ^{31}P MAS NMR spectra completely. Rather, with increasing Nb_2O_5 contents, a fourth component near −19 ppm can be identified, which increasingly contributes to the overall line shape. Based on this composition dependence, we attribute it to a Q^2 unit interacting with the niobium species in the structure. Consistent with the increasing contribution of this signal component the average chemical shift of the entire MAS-NMR spectrum moves gradually from −29 ppm, in the Nb_2O_5 free sample, towards −24 ppm in the sample with the highest Nb_2O_5 content, reflecting a monotonic change in the second coordination sphere of phosphorus.

Table 2
^{31}P NMR isotropic chemical shifts, δ_{iso}, Gaussian broadening, *lb*, area percentages obtained from lineshape deconvolutions. Note that for all the samples, the same chemical shift and line broadening parameters for the four individual deconvolution components were used. The numerals in the sample labels denote wt% of Nb_2O_5.

Sample	δ_{iso}/ ppm (± 0.2 ppm)			
	Q^1	$Q^{2'}$	Q^2	Q^3
	−10.8	−19.4	−27.9	−39.6
	lb / ppm (± 0.2 ppm)			
	15.6	14.2	19.6	17.5
	% (± 1%)			
PZABP	5	–	79	16
PZABP0	8	–	73	19
PZABP10	11	10	64	15
PZABP20	13	19	58	10
PZABP30	17	23	52	8

Fig. 4 shows the ^{27}Al MAS-NMR spectra, indicating the presence of four-, five- and six-coordinated Al in all the glasses. While the six-coordinated Al species are dominant in the niobium-free samples, Fig. 4 indicates a significant structural change as a function of composition: with increasing Nb_2O_5 content, the fraction of four-coordinate Al increases significantly, becoming the dominant environment in the sample containing 30 wt% of Nb_2O_5. The ^{27}Al isotropic chemical shifts are consistent with a second coordination sphere that is completely dominated by phosphate species. This conclusion is confirmed by the $^{27}Al\{^{31}P\}$ rotational echo double resonance (REDOR) results summarized in Fig. 5, which show comparable dipolar second moments $M_{2(Al-P)}$ to those measured in the model compound $AlPO_4$.

Fig. 6 shows ^{93}Nb MAS-NMR spectra of the Nb_2O_5-containing samples under study, revealing three featureless central transition components flanked by low-intensity spinning-sidebands arising from the central transition ($m = \pm 1/2 \leftrightarrow m = \mp 1/2$) and numerous satellite

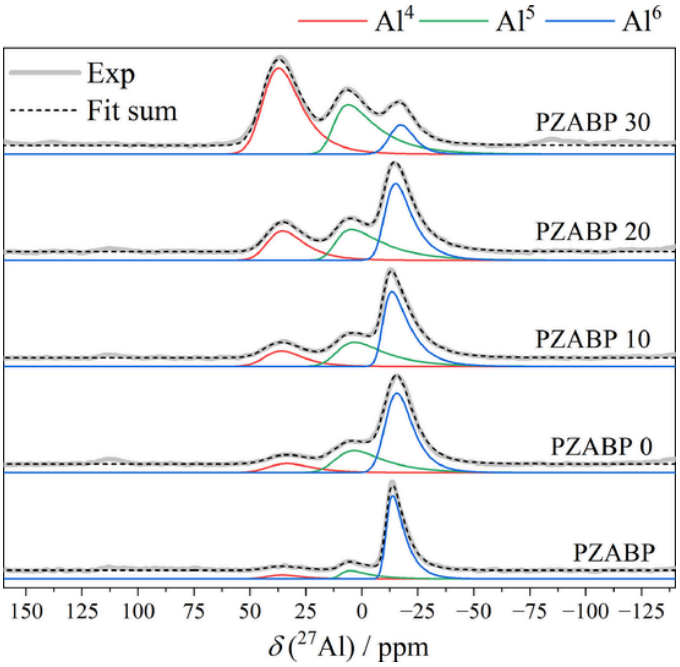

Fig. 4. ^{27}Al MAS NMR spectra of the samples under study. Fits to the data using the Czjzek distribution model are shown as dashed curves; the three components due to Al^4, Al^5, and Al^6 units are shown in red, green, and blue, respectively. The notations PZABP and PZABP 0 refer to rare-earth free and rare-earth doped base glasses. The numerals in the other sample labels denote wt% of Nb_2O_5.

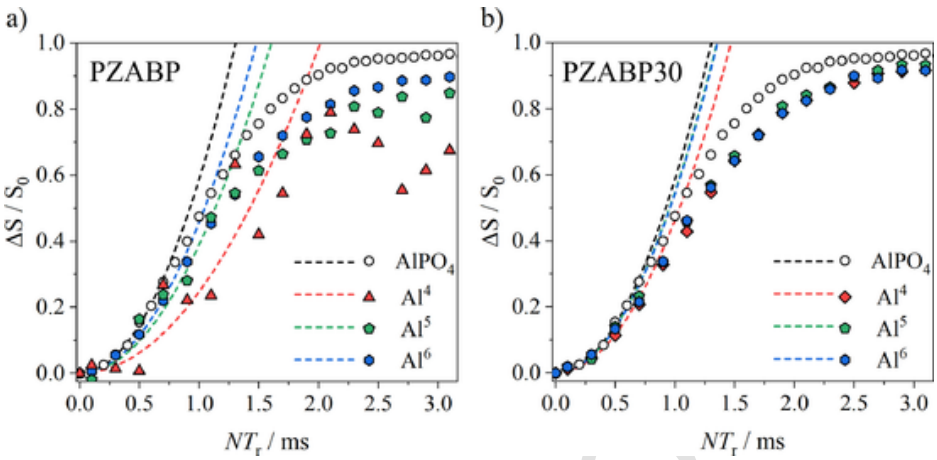

Fig. 5. $^{27}Al\{^{31}P\}$ REDOR dephasing curves of PZABP (a)) and PZABP30 (b)) together with crystalline $AlPO_4$. The black, red, green, and blue curves show parabolic fits to the data up to dephasing of $\Delta S/S_0 = 0.2$ for $AlPO_4$, and the Al^4, Al^5, and Al^6 units, in the glasses.

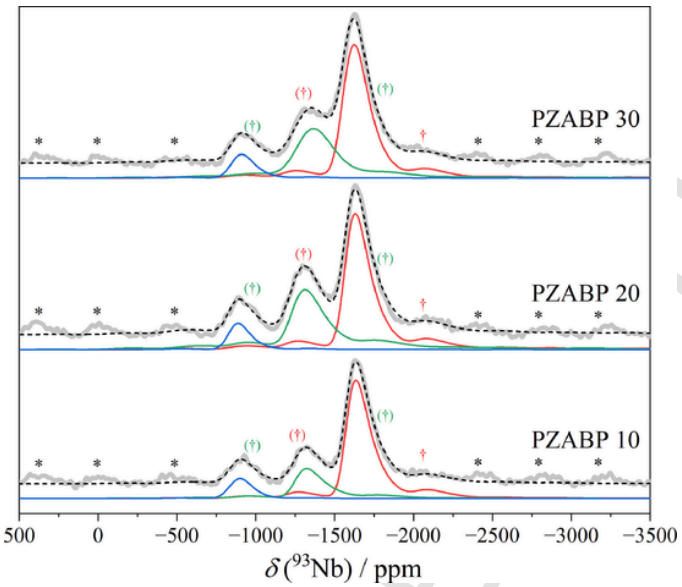

Fig. 6. ^{93}Nb rotor-synchronized Hahn-spinecho MAS NMR spectra of the samples under study. Asterisks and daggers mark spinning sidebands from satellite transitions and central transitions, respectively, while parentheses indicate the overlap of central transitions with central transition spinning sidebands. The numerals in the sample labels denote wt% of Nb_2O_5. Colored curves denote simulations of the central transitions of the three distinct niobium sites observed, using the Czjzek model of a wide distribution of quadrupolar coupling constants.

transitions ($\pm m \leftrightarrow \pm(m \pm 1)$), with $m = \{3/2, 5/2, 7/2, 9/2\}$). Compared to ^{93}Nb NMR spectra of Nb_2O_5-containing glasses found in early [25–34] and contemporary [23,35–37] works, the beneficial combination of the rather high magnetic field of 14.1 T and very fast MAS (60 kHz) allows for an unprecedentedly high resolution. Thus, for the first time – to the best of our knowledge – three distinct ^{93}Nb local environments can be evidenced in glasses with peak-to-peak resolution. The CT components can be well simulated by Czjzek distributions [38] of quadrupolar interaction parameters; see Table SI-3. While in Nb-containing oxide glasses mostly Nb in six-coordination is evidenced with isotropic chemical shifts near −1200 ppm, in the present case shifts near −840, −1250, and −1555 ppm are found. Concerning the high-frequency component, A, systematic work on crystalline Nb compounds [39] reports four and five-coordinated Nb sites to resonate with isotropic chemical shifts between −650 and −950 ppm, and −920 and −990 ppm respectively; for the former units rather high quadrupole coupling constants above 70 MHz have been reported. In the present case, the Czjzek fits suggest average quadrupolar product (P_Q) values of about 35 MHz, situated closer to five-coordinated Nb sites, ranging from 10 to 50 MHz. The isotropic chemical shift of about −1250 ppm observed for component B is typical for Nb in six coordination as it is seen in many oxide glasses and crystalline Nb_2O_5. Finally, the chemical shift of component C falls in the region of Nb in seven-coordination, while quadrupolar coupling constants are similar to those of NbO_6 units. In fact, in cases where the second Nb coordination sphere is dominated by other heteroatoms such as P or Ge, lower chemical shifts are observed, and in Nb_2O_5—$NaPO_3$ glasses, a component resonating near −1500 ppm was previously assigned to NbO_6 units [29,40]. Fig. 6 indicates further that the spectra are only weakly dependent on niobium contents. For specific peak assignments to structural Nb-containing units, additional work on crystalline niobium phosphate model compounds and interaction-selective 2D experiments will be necessary, as well as ab-initio calculations. All the NMR parameters extracted from NMR and REDOR analysis are summarized in Tables SI 1–SI 3.

Optical properties

Room temperature optical reflectance spectra of $Er^{3+}/Yb^{3+}/Eu^{3+}$ present in the glasses are shown in Fig. 7(A). The absorption peaks in the reflectance spectra centered at 376, 380, and 393 nm are attributed to the transitions from the ground state $^7F_0$ to the higher excited states $^5D_4$, $^5G_2$, and $^5L_6$, of the Eu^{3+} ions. These 4f → 4f intraconfigurational transitions are not allowed by Laporte's rule, and are observed due to the relaxation of this rule, occurring for example via vibronic coupling [19,41].

The absorption at wavelengths below 350 nm observed in all reflectance spectra of the glasses studied here is a characteristic of the PZABP glass matrix assigned to the oxygen ligand to metal (L→M) energy transfer involving the 2p orbital of the ligand and the 4f orbitals of Eu^{3+}, Er^{3+}, Yb^{3+} ions. Tauc's theory [42] was applied to obtain the band gap (E_g) values based on the experimental reflectance spectra for each material. The band gap values obtained shift monotonically to lower energy (3.98; 3.80; 3.68 and 3.55 eV) with increasing Nb_2O_5 concentration from zero to 30 wt%. The results presented in Fig. 7(A) and (B) are in agreement with the degree of glass transparency observed with the naked eye in the materials obtained. With increasing Nb_2O_5 content, a darkening of the glasses along with a loss in transparency is detected (Fig. SI 2)). This behavior is related to the increase in molar absorption, which is dependent on the concentration of Nb_2O_5 present

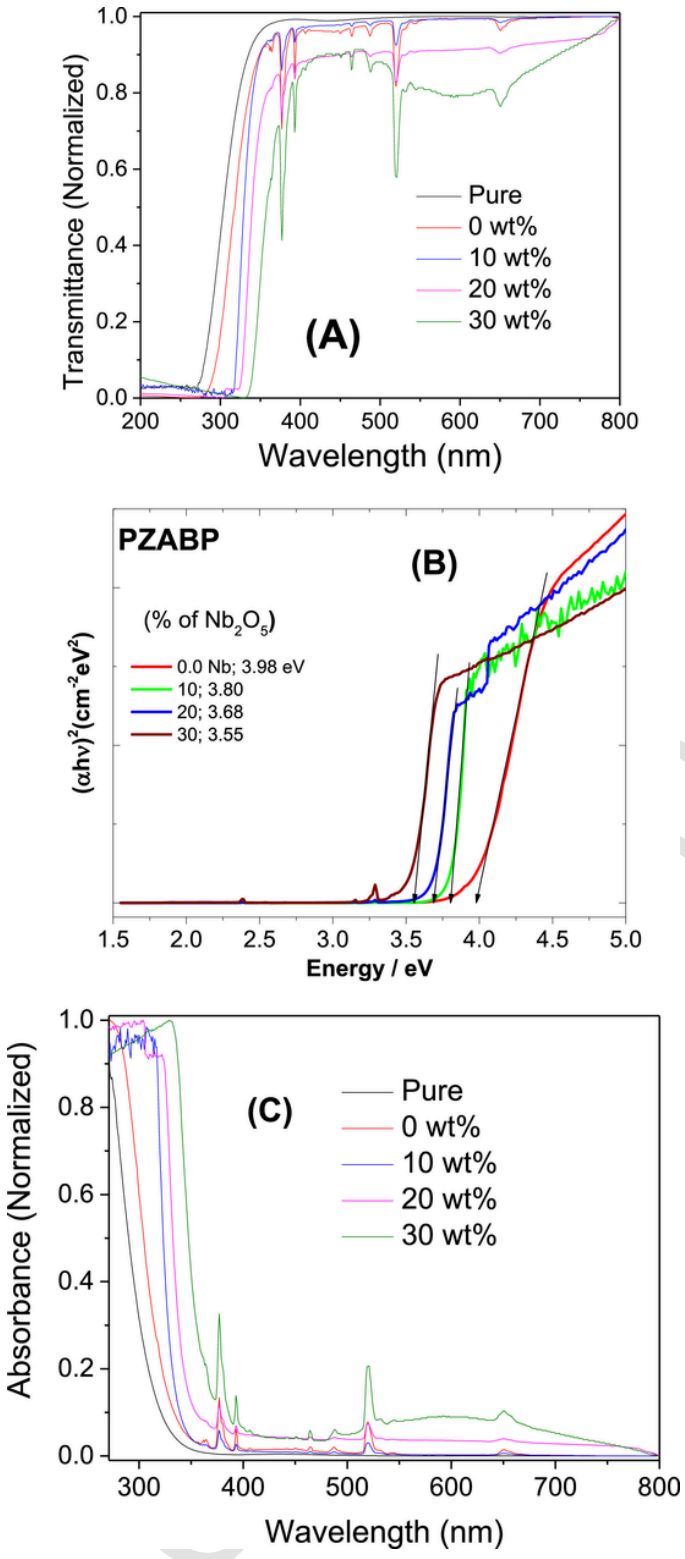

Fig. 7. (A) Room temperature Reflectance spectra of a pure undoped PZABP glass sample and glass samples doped with 1.0, 1.2, and 0.3 wt% of Eu_2O_3, Yb_2O_3 and Er_2O_3, respectively, containing 0.0, 10, 20, and 30 wt% Nb_2O_5, (B) Tauc's plot to calculate the band gap and (C) UV–Vis spectra for the rare-earth doped samples.

in the glasses. In addition, increasing Nb_2O_5 content produces a shift of the band edge to lower energies, leading to a decrease in the value of E_g [19,43]. In addition, some Nb^{4+} species may be present, and the blue coloration observed in some high-Nb glasses might arise from $Nb^{5+} \leftrightarrow Nb^{4+}$ intervalence transfer. However, no corresponding absorption band is observed, possibly as a result of the overall low transmission or because the coloration is an interference or scattering phenomenon associated with the non-transparent fraction of the material. The presence of the absorption band located between 500 and 700 nm, Fig. 7(C), for glass containing 30 wt% of Nb_2O_5, is associated with the observed coloration. To document the electronic structure of the glass and its possible effect on the luminescence of the RE^{3+} ions, the energy differences between direct and indirect bandgaps and the Urbach energy are summarized in Table 3.

In a study by Rego-Filho using a similar vitreous system based on PZABP co-doped with Yb^{3+}/Tm^{3+}, and applying the Davis-Mott model, a band gap energy (E_g) of 3.91 eV was obtained for an undoped sample. This value is close to those calculated from the data in the present study, which was 3.73 eV of the direct band gap and 3.75 eV of the indirect bandgap. Furthermore, the incorporation of the RE^{3+} ions into the previously reported glasses also led to a decrease in the band gap to 3.19 eV in the direct band gap and 3.14 eV in the indirect band gap. Despite the change in the band gap of the samples studied, it is only 14.9% lower than that found for the sample not containing Nb_2O_5. This slight change indicates that higher concentrations of doping can be accommodated in the PZABP matrix without dramatic changes to its overall electronic structure.

Urbach's theory [44] was applied to assess the degree of disorder exerted on the electronic structure of PZABP glass by the introduction of Nb_2O_5.The Urbach energy decreases to 0.12 eV with Nb_2O_5 levels of 10 wt%, then increases to 0.33 eV for 30 wt%, indicating that higher amounts of Nb_2O_5 increase the degree of disorder in the electronic structure, as shown in Fig. SI 3 and Table 3. This behavior is similar to that observed in borate glasses where Urbach energy values in the range between 0.12 and 0.22 eV were observed, reflecting an increase in the degree of disorder with increasing Nb_2O_5 content [45]. This behavior was the opposite of that observed by Senthil, who worked with tellurite glasses of composition TeO_2 –BaO–SrO–Nb_2O_5, for which the increase in the amount of Nb_2O_5 in the materials produced lower Urbach energies [45].

Fig. 8 indicates that a nephelauxetic effect, verified by the increase in optical basicity calculated from the work reported by Duffy and Ingram [46], occurs upon increasing Nb_2O_5 content. With increasing Nb_2O_5 concentration the electronic density distribution of the oxygen atoms is modified. The optical basicity values used of each oxide present in PZAPB glass composition were: Nb_2O_5 = 1.05, P_2O_5 = 0.33, ZnO = 1.03, Al_2O_3 = 0.6, BaO = 1.21, PbO = 1.19, Yb_2O_3 = 0.893, Eu_2O_3 = 0.976 and Er_2O_3 = 0.929 [47]. The polarization of oxygen in the structure promotes this species as a Lewis base. Based on the indirect band gap values (E_g), the optical electronegativity was calculated from Duffy's equation [48] $\Lambda_{opt} = 0.2688 \times E_g$, see Table 3.

Table 4 lists the refractive index values measured at three different wavelengths using the prism coupling technique. They increase as a function of Nb_2O_5 content. This is expected, because the refractive index increment value of the Nb_2O_5 component is higher than that of all the other oxides present in the glass. The profiles of refractive index as a function of wavelength are shown in Fig. SI 4. (see Table 4).

The excitation spectra, monitoring the emission intensity via the $^5D_0 \rightarrow {}^7F_2$ transition of Eu^{3+} (612 nm), in the spectral range from 250 to 500 nm showed similar bands even with increasing concentrations of Nb_2O_5 at room temperature, Fig. 9(A). The $^7F_0 \rightarrow {}^5L_6$ transition (392.5 nm) presents the highest intensity band of the intraconfigurational transitions.

The emission spectra of PZABP materials can be seen in Fig. 9(B) under excitation in the Eu^{3+} band ($^7F_0 \rightarrow {}^5L_6$) at 392.5 nm, recorded in the range 550–750 nm. Table 5 lists the ratio of the integrated areas of the transitions $^5D_0 \rightarrow {}^7F_2$/ $^5D_0 \rightarrow {}^7F_1$, which correlates with the extent of covalency, reflecting the asymmetry of the ligand environment [49–51].

Table 3
Optical Basicity (Λg) calculated based on the Duffy and Ingram [46] theory, Optical electronegativity (χ_{opt}), direct and indirect band gap values and the difference Δ between them calculated based on the Tauc equation and Urbach energy *UE* using the experimental UV–vis spectra data of each oxide in the composition of the glass as a function of Nb_2O_5 concentration. All energies are given in units of eV.

		Composition of the glass and optical and basicity parameters extracted from the experimental data												
(Λg)	χ_{opt}	Nb_2O_5	P_2O_5	ZnO	Al_2O_3	BaO	PbO	Yb_2O_3	Eu_2O_3	Er_2O_3	Direct band-gap (D)	Indirect band-gap (I)	Δ	*UE**
0.6418	1.0080	0	59.30	8.50	3.55	10.67	15.54	1.2	1.0	0.3	3.73	3.75	0.02	0.22
0.6827	0.9730	10	53.33	7.65	3.20	9.60	13.99	1.1	0.9	0.27	3.69	3.62	0.07	0.12
0.7249	0.9435	20	47.77	6.80	2.84	8.54	12.43	1.0	0.8	0.24	3.48	3.51	0.03	0.16
0.7643	0.8440	30	41.51	5.95	2.49	7.47	10.88	0.84	0.7	0.21	3.19	3.14	0.05	0.33

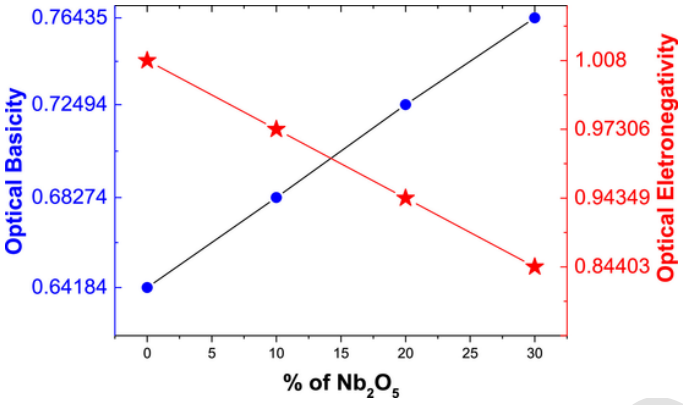

Fig. 8. Optical basicity and optical electronegativity as a function of Nb_2O_5 wt percentage in the PZABP glass samples doped with 1.0, 1.2, and 0.3 wt% of Eu_2O_3, Yb_2O_3 and Er_2O_3 respectively, containing Nb_2O_5 at levels of 0.0, 10, 20, and 30 wt%.

Table 4
Refractive index of PZABP glass samples with 1.0, 1.2, and 0.3 wt% of Eu_2O_3, Yb_2O_3 and Er_2O_3, respectively, containing Nb_2O_5 at levels of 0.0, 10, 20, and 30 wt% at 532.8; 632.8 and 1538 nm for TE and TM modes. (the profile of the refractive index as a function of Nb_2O_5 content and wavelength can be verified in the Fig. SI 4.).

	Refractive Index					
wt% of Nb_2O_5	532.8 nm		632.8 nm		1538 nm	
	TE	TM	TE	TM	TE	TM
PZABP	1.5844	1.5847	1.5906	1.5908	1.5685	1.5683
0	1.5927	1.5923	1.5859	1.5856	1.5686	1.5650
10	1.6223	1.6229	1.6160	1.6159	1.5959	1.5958
20	1.6544	1.6544	1.6430	1.6428	1.6207	1.6207
30	1.6796	1.6796	1.6688	1.6683	1.6439	1.6435

The ratio tends to decrease slightly from 4.17 to 3.25 with increasing Nb_2O_5 content, suggesting gradual changes in the local environment of the Eu^{3+} ions towards less covalent or more symmetric electron density distributions. This change leads to a diminution of the value of the relevant Judd-Ofelt parameter governing the luminescence emission cross-section of the electric dipole-allowed $^5D_0 \rightarrow {}^7F_2$ transition.

The Eu^{3+} lifetime values were recorded by monitoring the $^5D_0 \rightarrow {}^7F_2$ transition (612 nm) under excitation at 392.5 nm, assigned to the $^7F_0 \rightarrow {}^5L_6$ transition, Fig. 10. The curves were fitted according to a bi-exponential decay yielding the parameters listed in Table 5. We note that the bi-exponential model is only one of multiple possibilities of fitting the data; it is consistent with the presence at least two distinct emitting species with different lifetimes. An alternative would be a stretched exponential reflecting a continuous distribution of lifetimes or the average excited-state lifetime values $<\tau>$ at which the emission intensity reached the fraction 1/e of the initial intensity value following pulsed excitation. Table 5 indicates that these $<\tau>$ values decrease from 2.17 to 1.62 ms with increasing concentration of Nb_2O_5. They are

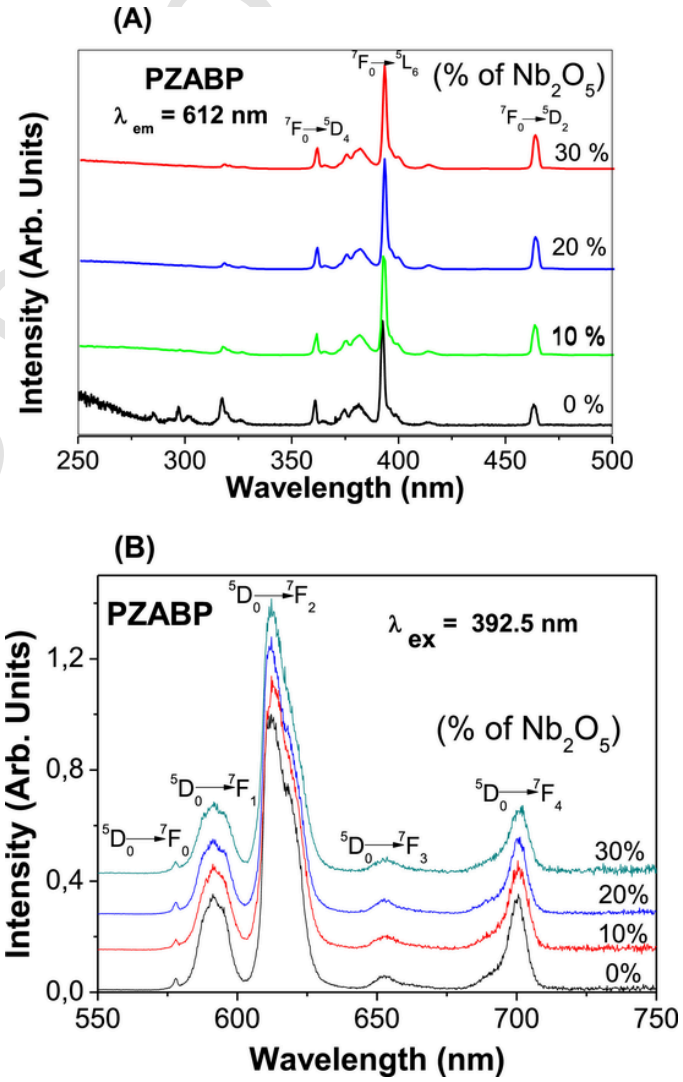

Fig. 9. (A) Eu^{3+} Room temperature excitation spectra monitoring emission at 612 nm, and (B) Room temperature Eu^{3+} emission spectra under excitation at 392.5 nm of the PZABP glass samples doped with 1.0, 1.2, and 0.3 wt% of Eu_2O_3, Yb_2O_3 and Er_2O_3, respectively, containing Nb_2O_5 at levels of 0.0, 10, 20, and 30 wt%.

like those reported in the literature for a phosphate glass system also doped with RE^{3+} ions in the presence of niobium [19]. The fitted decay lifetime curves are depicted in Fig. SI 5.

The results indicate that Nb_2O_5 tends to reduce rare-earth luminescence in PZABP glasses, due to stronger non-radiative processes and/or cross-relaxation and reduction of total lifetime values. Another point that must be considered is that increasing the amount of Nb_2O_5 (refractive index 2.35 at 632.8 nm) changes the values of the refractive index

Table 5
Ratio of the emission intensities of the electric dipole allowed transition $^5D_0 \rightarrow {}^7F_2$ and the magnetic dipole allowed $^5D_0 \rightarrow {}^7F_1$ transition as extracted from the room temperature Eu^{3+} emission spectra, lifetime values deduced from the bi-exponential decay analysis and from the time $<\tau>$ at which the emission intensity reached the fraction 1/e of the initial intensity value following pulsed excitation, under excitation at 392.5 nm, and position and FWHM of the emission band positioned around 1550 nm as a function of Nb_2O_5 percentage, present in the PZABP glass, under excitation at 980 nm.

wt% of Nb_2O_5	Ratio: $^5D_0 \rightarrow {}^7F_2/{}^5D_0 \rightarrow {}^7F_1$	t_1 (±0.1 ms)	t_2 (±0.1 ms)	τ (±0.1 ms)*	Maximum Emission Peak at 1532 nm of Er^{3+} (± 1 nm)	FWHM of band positioned at 1532 nm (± 1 nm)
0	4.17	0.7654	2.4314	2.1727	1535.0	30.7
10	3.64	0.8026	2.2354	1.9124	1534.8	23.3
20	3.24	0.8297	2.1080	1.8427	1535.2	20.5
30	3.25	0.6551	1.9038	1.6000	1534.6	23.5

* Time at which the emitted intensity has decreased to a value of 1/e times its initial intensity.

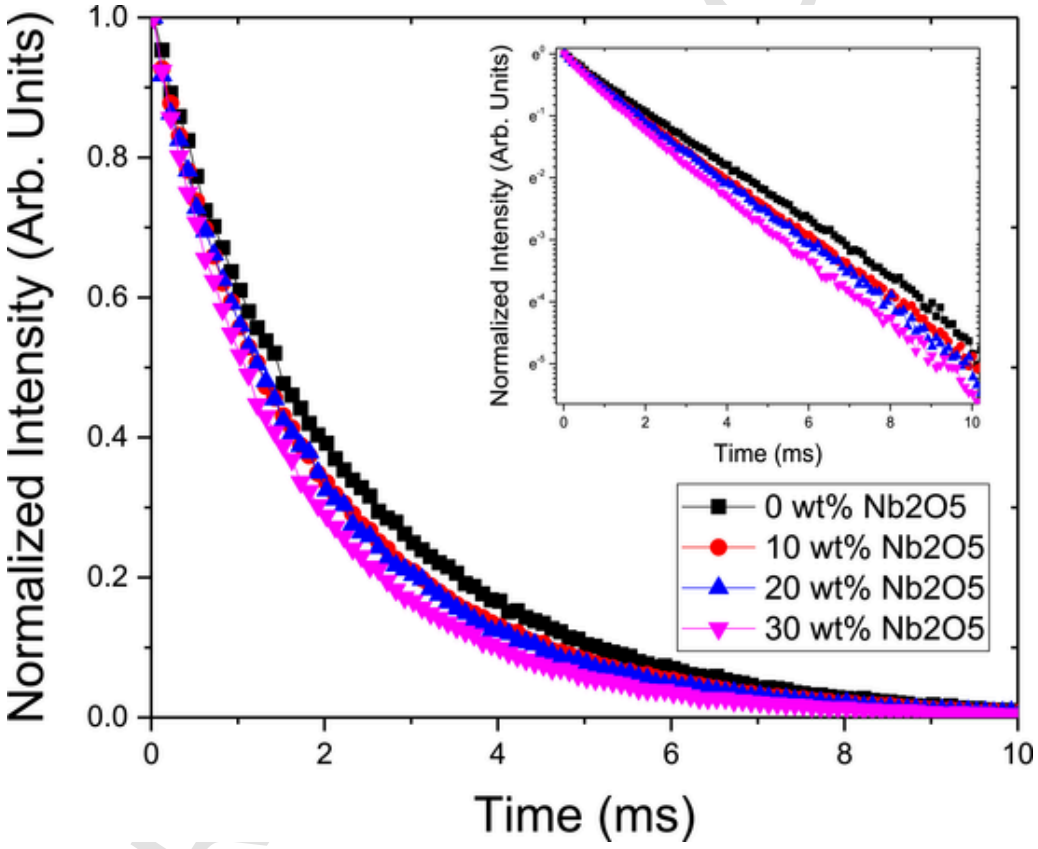

Fig. 10. Fluorescence decay of Eu^{3+} emission at 612 nm of the PZABP glass samples doped with 1.0, 1.2, and 0.3 wt% of Eu_2O_3, Yb_2O_3 and Er_2O_3, respectively, containing Nb_2O_5 at levels of 0.0, 10, 20, and 30 wt% upon pulsed excitation at 392.5 nm, respectively, as a function of Nb_2O_5 content. The inset presents the linearization of the exponential curve. All fitted decay curves are presented in Fig. SI 8.

of the medium, which can lead to a reduction in the lifetime values of the excited state [52–55].

Fig. SI 6 shows the emission bands verified in the region between 500 and 700 nm under excitation at 980 nm. They are attributed to the upconversion phenomenon present in the system using Yb^{3+} as a sensitizer in these samples. The emission bands located between 500 and 550 nm, 570 and 630 nm, and those between 630 and 700 nm are assigned to the transitions $^2H_{11/2} \rightarrow {}^4I_{15/2}$ (Er^{3+}), $^5D_0 \rightarrow {}^7F_2$ (Eu^{3+}) and $^4F_{9/2} \rightarrow {}^5I_{15/2}$ (Er^{3+}), respectively. These can occur through different mechanisms illustrated in Fig. SI 7. One of the suggested mechanisms for the emission in the green region could be the excitation of electrons from the $^4I_{15/2}$ state of Er^{3+} to the $^4I_{11/2}$ state of the same ion and further promotion from the $^4I_{11/2}$ state to the $^4F_{7/2}$ state of the same ion by a second photon. Subsequently, non-radiative decay mechanisms could occur to the $^2H_{11/2}$ and $^4S_{3/2}$ levels, promoting radiative decay to the $^4I_{15/2}$ ground state, producing green emission. An alternative mechanism may involve the Yb^{3+} ion as a sensitizer. Pumping at 980 nm promotes the simultaneous excitation of Er^{3+} and Yb^{3+} between levels $^4I_{15/2}$ to $^4I_{11/2}$ and from $^2F_{7/2}$ to $^2F_{5/2}$, respectively. Then the Yb^{3+} transfers energy to the Er^{3+} promoting the electron from the $^4I_{11/2}$ level to the $^4F_{7/2}$ level. Following non-radiative decay, as explained previously, green emission from the $^2H_{11/2}$ and $^4S_{3/2}$ levels would be observed.

Emissions in the range between 630 and 690 nm observed in Fig. SI 6 are assigned to the Er^{3+} ions, occurring from the $^4F_{9/2}$ energy levels, which can be populated via energy transfer from the Yb^{3+} ion or non-radiative decays from the $^4F_{7/2}$, $^2H_{11/2}$ and $^4S_{3/2}$ levels of the Er^{3+} ion. The emission bands positioned between 570 and 630 nm are attributed to hypersensitive $^5D_0 \rightarrow {}^7F_2$ emission of Eu^{3+}, that is enhanced via energy transfer from the Er^{3+} and/or Yb^{3+} ions. The proposed mechanism was also observed by Buarque et al. [56]

The graphs presented in Fig. SI 8 provide crucial information about the number of photons involved in the upconversion emission process, and the understanding of its possible mechanisms. The intensity of the upconversion emission bands is related to the excitation pumping

power according to the expression $I \alpha P^n$, where I is the integrated emission area, P is the excitation source power and n is the number of photons involved in the process of excitation [57–59]. In accordance with the results, the linear behavior observed in the double logarithmic plots for all samples presents slopes with values between 1.38 and 2.24, indicating that the numbers of absorbed photons are around 2; this suggests that the upconversion mechanisms of the material occur through the absorption of two photons.

The CIE coordinates obtained by the program SpectraChroma 1.0.1 [60] were based on their respective emission spectra. All the PZABP:Eu^{3+} samples show monochromatic emission in the visible-red region under excitation at 392.5 nm (Fig. SI 9), with only a minor influence of the Nb_2O_5 content on the emission maximum and linewidth. Furthermore, all emission spectra with excitation at 392 nm showed emission bands associated with transitions between Eu^{3+} energy levels.

The emission spectra in the infrared region between 1450 nm and 1650 nm of PZABP materials under excitation at 980 nm with 100 mW of pumping power are shown in Fig. 11. Samples showed intense emission in the near-infrared region, with a emission peak maximum centered around 1535 nm. This band is assigned to the $^4I_{13/2} \rightarrow {}^4I_{15/2}$ transition of the Er^{3+} ions [19,61,62]. Table 5 shows the central position and FWHM values. Higher FWHM values are found in samples with lower Nb_2O_5 percentages. The observed emission around 1550 nm can be associated with Er^{3+} ion emission, which may be excited by the laser at 980 nm as excitation source, or else the Yb^{3+} ions close by may be acting as sensitizers transferring energy to Er^{3+} promoting this emission. The possible mechanisms involved can be accompanied with reference to Fig. SI 7 in the Supporting Information.

4. Conclusions

Nb_2O_5 was successfully incorporated into RE^{3+}-doped phosphate glasses of the PZAPB system using the standard melt cooling method. The glasses were structurally characterized by Raman spectroscopy and by ^{31}P, ^{27}Al, and ^{93}Nb solid state NMR. With increasing Nb_2O_5 content the increased participation of niobium in the second phosphorus coordination sphere is reflected by a monotonic change in the ^{31}P chemical shift, and the appearance of a new site, characterized by P-O-Nb connectivity. Significant changes are also observed in the Al speciation: with increasing Nb_2O_5 content aluminum becomes increasingly four-coordinate. Furthermore, multiple Nb environments are resolved in the ^{93}Nb MAS-NMR spectra, possibly revealing sites with different coordination numbers. Optical reflectance and luminescence studies indicate that the RE^{3+} emission intensities and excited-state lifetimes are only moderately affected by Nb_2O_5 incorporation. Thus, the PZABP glass matrix reported here can be considered a promising candidate as a host for photonic devices. The refractive index can be fine-tuned via the Nb_2O_5 content, to meet requirements for specific applications. Also, incorporation of Nb_2O_5 does not affect significantly the up- and downshifting processes involving the RE^{3+} dopants.

In addition, it is suggested that these glasses can be applied in UV filters, UV and IV band energy converters for visible, and even for application in optical fibers in the 3rd Telecom window.

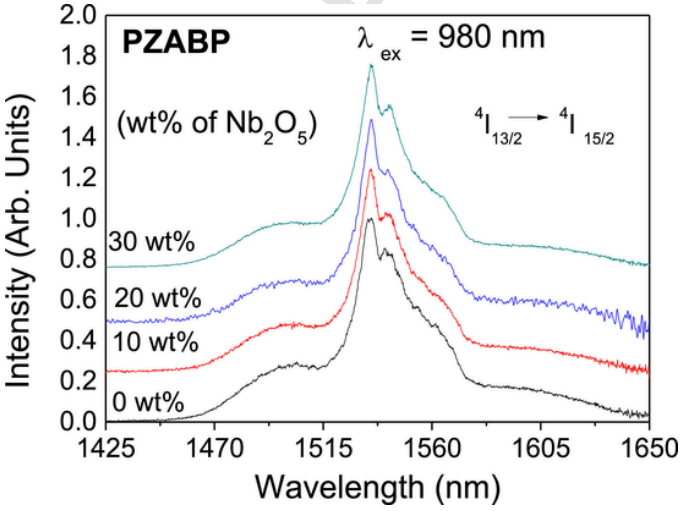

Fig. 11. Emission spectra under laser excitation at 980 nm, at room temperature, of PZABP glass samples doped with 1.0, 1.2, and 0.3 wt% of Eu_2O_3, Yb_2O_3 and Er_2O_3, respectively, containing Nb_2O_5 at levels of 0.0, 10, 20, and 30 wt%.

CRediT authorship contribution statement

José Henrique Faleiro : Conceptualization, Methodology, Investigation, Resources, Writing – review & editing, Visualization. **Noelio O. Dantas :** Methodology, Investigation, Resources, Writing – review & editing, Visualization. **Anielle C.A. Silva :** Methodology, Investigation, Resources, Writing – review & editing, Visualization. **Helliomar P. Barbosa :** Conceptualization, Investigation, Resources, Writing – review & editing. **Bruno H.S.T. da Silva :** Conceptualization, Investigation, Resources, Writing – review & editing. **Karmel de O. Lima :** Conceptualization, Investigation, Resources, Writing – review & editing. **Guilherme de Freitas Silva :** Conceptualization, Investigation, Resources, Writing – review & editing. **Rogéria Rocha Gonçalves :** Conceptualization, Investigation, Resources, Writing – review & editing. **Rodrigo Falci :** Conceptualization, Investigation, Resources, Writing – review & editing. **Younès Messadeq :** Investigation, Resources, Writing – review & editing. **Isabela Dias de Oliveira Branco :** Conceptualization, Methodology, Investigation, Resources, Writing – review & editing, Visualization. **Bianca M. Cerrutti :** Conceptualization, Methodology, Investigation, Resources, Writing – review & editing, Visualization. **Henrik Bradtmüller :** Conceptualization, Investigation, Resources, Writing – review & editing, Visualization. **Hellmut Eckert :** Conceptualization, Methodology, Investigation, Resources, Writing – review & editing, Visualization. **Jefferson Luis Ferrari :** Conceptualization, Methodology, Supervision, Investigation, Resources, Writing – review & editing, Project administration, Funding acquisition.

Declaration of Competing Interest

The authors declare that they have no known competing financial interests or personal relationships that could have appeared to influence the work reported in this paper.

Data availability

No data was used for the research described in the article.

Acknowledgments

The authors would like to acknowledge FAPEMIG, FAPESP (Project Numbers: 2020/05319-9, 2018/18213-4, 2013/07793-6, 2019/26399-3), FINEP, and CNPq. This work is a collaboration research project of members of the Rede Mineira de Química (RQ-MG) supported by FAPEMIG. This study was financed in part by the Coordenação de Aperfeiçoamento de Pessoal de Nível Superior - Brasil (CAPES) - Finance Code 001. The authors thank Companhia Brasileira de Metalurgia e Mineração (CBMM) for donating of Nb_2O_5 added in the preparation of materials. Prof. Jefferson L. Ferrari acknowledges UFU/CAPES/PRINT funding for carrying out work at Laval University.

Supplementary materials

Supplementary material associated with this article can be found, in the online version, at doi:10.1016/j.jnoncrysol.2023.122173.

References

[1] A. Zakery, S.R. Elliott, Optical Nonlinearities in Chalcogenide Glasses and Their Applications, Springer, 2007.

[2] M.K. Halimah, M.F. Faznny, M.N. Azlan, H.A.A. Sidek, Optical basicity and electronic polarizability of zinc borotellurite glass doped La^{3+} ions, Results Phys. 7 (2017) 581–589, https://doi.org/10.1016/j.rinp.2017.01.014.

[3] C.R. Kesavulu, A.C. Almeida Silva, M.R. Dousti, N.O. Dantas, A.S.S. de Camargo, T. Catunda, Concentration effect on the spectroscopic behavior of Tb^{3+} ions in zinc phosphate glasses, J. Lumin. 165 (2015) 77–84, https://doi.org/10.1016/j.jlumin.2015.04.012.

[4] J.A. Wilder, Glasses and glass ceramics for sealing to aluminum alloys, J. Non Cryst. Solids 38–39 (1980) 879–884, https://doi.org/10.1016/0022-3093(80)90548-7.

[5] A.U. Trápala-Ramírez, J.L.N. Gálvez-Sandoval, A. Lira, I. Camarillo, E. Alvarez-Ramos, A.N. Meza-Rocha, U. Caldiño, Calcium-zinc phosphate glasses activated with Tb^{3+}/Eu^{3+} for laser and white LED applications, J. Lumin. 215 (2019) 116621, https://doi.org/10.1016/j.jlumin.2019.116621.

[6] C.R. Kesavulu, K.K. Kumar, N. Vijaya, K.S. Lim, C.K. Jayasankar, Thermal, vibrational and optical properties of Eu^{3+}-doped lead fluorophosphate glasses for red laser applications, Mater. Chem. Phys. 141 (2013) 903–911, https://doi.org/10.1016/j.matchemphys.2013.06.021.

[7] B. Tischendorf, J.U. Otaigbe, J.W. Wiench, M. Pruski, B.C. Sales, A study of short and intermediate range order in zinc phosphate glasses, J. Non Cryst. Solids 282 (2001) 147–158, https://doi.org/10.1016/S0022-3093(01)00350-7.

[8] B. Zhang, Q. Chen, L. Song, H. Li, F. Hou, J. Zhang, Fabrication and properties of novel low-melting glasses in the ternary system $ZnO–Sb_2O_3–P_2O_5$, J. Non Cryst. Solids 354 (2008) 1948–1954, https://doi.org/10.1016/j.jnoncrysol.2007.11.007.

[9] N.O. Dantas, E.S.F. Neto, R.S. Silva, D.R. Jesus, F. Pelegrini, Evidence of $Cd_{1-x}Mn_xS$ nanocrystal growth in a glass matrix by the fusion method, Appl. Phys. Lett. 93 (2008) 193115, https://doi.org/10.1063/1.3027471.

[10] H. Nurhafizah, Z.A.S. Nurulwahidah, M.D.A. Nazihah, A.N. Hidayah, Effects of Ag NPs: enhancement of mechanical properties of Er^{3+}/Nd^{3+} codoped lithium niobate tellurite glass via ultrasonic measurement, J. Phys. Conf Ser. (2021) 12035 IOP Publishing.

[11] N.A. Wójcik, S. Ali, E.I. Kamitsos, D. Möncke, Niobate in silicate and phosphate glasses: effect of glass basicity on crucible dissolution, Int. J. Appl. Glass Sci. 13 (2022) 121–134, https://doi.org/10.1111/ijag.16505.

[12] R.F. Falci, T.C. Ranquine, N.O. Dantas, V. Anjos, M.J.V. Bell, Upconversion and near infrared emission in Yb–Tm mediated by ZnTe crystals in oxide glasses, Opt. Mater. 124 (2022), 111843 https://doi.org/10.1016/j.optmat.2021.111843 (Amst).

[13] R. Ulrich, R. Torge, Measurement of thin film parameters with a prism coupler, Appl. Opt. 12 (1973) 2901, https://doi.org/10.1364/AO.12.002901.

[14] T. Gullion, J. Schaefer, Rotational-echo double-resonance NMR, J. Magn. Reson. 81 (1969) (1989) 196–200, https://doi.org/10.1016/0022-2364(89)90280-1.

[15] M. Bertmer, H. Eckert, Dephasing of spin echoes by multiple heteronuclear dipolar interactions in rotational echo double resonance NMR experiments, Solid State Nucl. Magn. Reson. 15 (1999) 139–152, https://doi.org/10.1016/S0926-2040(99)00050-8.

[16] J.C.C. Chan, H. Eckert, Dipolar coupling information in multispin systems: application of a compensated REDOR NMR approach to inorganic phosphates, J. Magn. Reson. 147 (2000) 170–178, https://doi.org/10.1006/jmre.2000.2191.

[17] D. Massiot, F. Fayon, M. Capron, I. King, S. le Calvé, B. Alonso, J.O. Durand, B. Bujoli, Z. Gan, G. Hoatson, Modelling one- and two-dimensional solid-state NMR spectra, Magn. Reson. Chem. 40 (2002) 70–76, https://doi.org/10.1002/mrc.984.

[18] J. Kuczek, P. Jeleń, J. Sułowska, M. Szumera, Correlation between glass transition effect and structural changes in multicomponent iron phosphate-silicate glasses, J. Therm. Anal. Calorim. 138 (2019) 4145–4153, https://doi.org/10.1007/s10973-019-08465-5.

[19] J.H. Faleiro, N.O. Dantas, A.C.A. Silva, H.P. Barbosa, B.H.S.T. da Silva, K. de O. Lima, R.R. Gonçalves, J.L. Ferrari, Niobium oxide influence in the phosphate glasses triply doped with $Er^{3+}/Yb^{3+}/Eu^{3+}$ prepared by the melting process, J. Non Cryst. Solids 571 (2021) 121051, https://doi.org/10.1016/j.jnoncrysol.2021.121051.

[20] A.K. Yadav, P. Singh, A review of the structures of oxide glasses by Raman spectroscopy, RSC Adv. 5 (2015) 67583–67609, https://doi.org/10.1039/C5RA13043C.

[21] I. Soltani, S. Hraiech, K. Horchani-Naifer, H. Elhouichet, B. Gelloz, M. Férid, Growth of silver nanoparticles stimulate spectroscopic properties of Er^{3+} doped phosphate glasses: heat treatment effect, J. Alloy. Compd. 686 (2016) 556–563, https://doi.org/10.1016/j.jallcom.2016.06.027.

[22] G. Monteiro, L.F. Santos, J.C.G. Pereira, R.M. Almeida, Optical and spectroscopic properties of germanotellurite glasses, J. Non Cryst. Solids 357 (2011) 2695–2701, https://doi.org/10.1016/j.jnoncrysol.2010.12.062.

[23] L.M. Marcondes, S. Maestri, B. Sousa, R.R. Gonçalves, F.C. Cassanjes, G.Y. Poirier, High niobium oxide content in germanate glasses: thermal, structural, and optical properties, J. Am. Ceram. Soc. 101 (2018) 220–230, https://doi.org/10.1111/jace.15215.

[24] Y. Takahashi, H. Masai, M. Osada, T. Fujiwara, Precursive stage of nanocrystallization in niobium oxide-containing glass, Appl. Phys. Lett. 95 (2009) 71909, https://doi.org/10.1063/1.3211989.

[25] T. Otsuka, M.R. Cicconi, D. Dobesh, B. Schroeder, T. Hayakawa, Nb NMR study of (K, Na)NbO3-doped SiO2-Na2O-Al2O3 glasses, (2022). 10.1002/pssb.202200016.

[26] U. Hoppe, L. Delevoye, L. Montagne, M.V. Zimmermann, A.C. Hannon, Structure of Nb_2O_5-$NaPO_3$ glasses by X-ray and neutron diffraction, Phys. Chem. Chem. Phys. 15 (2013) 8520, https://doi.org/10.1039/c2cp42772a.

[27] S. Chenu, U. Werner-Zwanziger, C. Calahoo, J.W. Zwanziger, Structure and properties of $NaPO_3–ZnO–Nb_2O_5–Al_2O_3$ glasses, J. Non Cryst. Solids 358 (2012) 1795–1805, https://doi.org/10.1016/J.JNONCRYSOL.2012.05.027.

[28] J. v Hanna, K.J. Pike, T. Charpentier, T.F. Kemp, M.E. Smith, B.E.G. Lucier, R.W. Schurko, L.S. Cahill, A 93 Nb solid-state NMR and density functional theory study of four-and six-coordinate niobate systems, (n.d.) 2023. 10.1002/chem.200901581.

[29] A. Flambard, J.J. Videau, L. Delevoye, T. Cardinal, C. Labrugère, C.A. Rivero, M. Couzi, L. Montagne, Structure and nonlinear optical properties of sodium–niobium phosphate glasses, J. Non Cryst. Solids 354 (2008) 3540–3547, https://doi.org/10.1016/J.JNONCRYSOL.2008.03.017.

[30] D. Khabibulin, K. Romanenko, M. Zuev, O. Lapina, Solid state NMR characterization of individual compounds and solid solutions formed in Sc_2O_3-V_2O_5-Nb_2O_5-Ta_2O_5 system, Magn. Reson. Chem. 45 (2007) 962–970, https://doi.org/10.1002/mrc.2086.

[31] A. Flambard, L. Montagne, L. Delevoye, S. Steuernagel, ^{93}Nb and ^{17}O NMR chemical shifts of niobiophosphate compounds, Solid State Nucl. Magn. Reson. 32 (2007) 34–43, https://doi.org/10.1016/J.SSNMR.2007.07.001.

[32] K.O. Drake, D. Carta, L.J. Skipper, F.E. Sowrey, R.J. Newport, M.E. Smith, A multinuclear solid state NMR study of the sol–gel formation of amorphous $Nb_2O_5–SiO_2$ materials, Solid State Nucl. Magn. Reson. 27 (2005) 28–36, https://doi.org/10.1016/J.SSNMR.2004.08.008.

[33] A. Flambard, L. Montagne, L. Delevoye, G. Palavit, J.P. Amoureux, J.J. Videau, Solid-state NMR study of mixed network sodium–niobium phosphate glasses, J. Non Cryst. Solids 345–346 (2004) 75–79, https://doi.org/10.1016/J.JNONCRYSOL.2004.07.046.

[34] R.T. Hart, M.A. Anspach, B.J. Kraft, J.M. Zaleski, J.W. Zwanziger, P.J. DeSanto, B. Stein, J. Jacob, P. Thiyagarajan, Optical implications of crystallite symmetry and structure in potassium niobate tellurite glass ceramics, Chem. Mater. 14 (2002) 4422–4429, https://doi.org/10.1021/cm020615q.

[35] P. Kalenda, L. Koudelka, P. Mošner, L. Montagne, B. Revel, J. Trebosc, Glass to crystal transformation in the ternary $BaO-Nb_2O_5-P_2O_5$ system, J. Mol. Struct. 1143 (2017) 472–477, https://doi.org/10.1016/J.MOLSTRUC.2017.04.112.

[36] M. Dolhen, M. Allix, V. Sarou-Kanian, F. Fayon, C. Genevois, S. Chenu, P.E. Coulon, M. Colas, J. Cornette, J.R. Duclère, F. Brisset, O. Masson, P. Thomas, G. Delaizir, A comprehensive study of the glass/translucent anti-glass/transparent ceramic structural ordering in the $Bi_2O_3-Nb_2O_5–TeO_2$ system, Acta Mater. 189 (2020) 73–84, https://doi.org/10.1016/J.ACTAMAT.2020.02.062.

[37] D.L. Costa-silva, J.F. Bartolomé, A.C. Silva, S. Mello-Castanho, Structural and thermal influence of niobia in aluminoborosilicate glasses, Ceram. Int. 48 (2022) 18433–18440, https://doi.org/10.1016/J.CERAMINT.2022.03.112.

[38] G. Czjzek, J. Fink, F. Götz, H. Schmidt, J.M.D. Coey, J.P. Rebouillat, A. Liénard, Atomic coordination and the distribution of electric field gradients in amorphous solids, Phys. Rev. B 23 (1981) 2513–2530, https://doi.org/10.1103/PhysRevB.23.2513.

[39] O.B. Lapina, D.F. Khabibulin, K.V. Romanenko, Z. Gan, M.G. Zuev, V.N. Krasil'nikov, V.E. Fedorov, ^{93}Nb NMR chemical shift scale for niobia systems, Solid State Nucl. Magn. Reson. 28 (2005) 204–224, https://doi.org/10.1016/j.ssnmr.2005.09.003.

[40] L.M. Marcondes, H. Bradtmüller, S.N. Carvalho dos Santos, L.K. Nolasco, C.R. Mendonça, S.H. Santagneli, G.Y. Poirier, M. Nalin, Structural and luminescence characterization of europium-doped niobium germanate glasses and glass-ceramics: novel insights from ^{93}Nb solid-state NMR spectroscopy, Ceram. Int. 48 (2022) 20801–20808, https://doi.org/10.1016/J.CERAMINT.2022.04.062.

[41] J.B. Prasannakumar, Y.S. Vidya, K.S. Anantharaju, G. Ramgopal, H. Nagabhushana, S.C. Sharma, B.D. Prasad, S.C. Prashantha, R.B. Basavaraj, H. Rajanaik, Bio-mediated route for the synthesis of shape tunable $Y_2O_3:Tb^{3+}$ nanoparticles: photoluminescence and antibacterial properties, Spectrochim. Acta A Mol. Biomol. Spectrosc. 151 (2015) 131–140, https://doi.org/10.1016/j.saa.2015.06.081.

[42] J. Tauc, Optical properties and electronic structure of amorphous Ge and Si, Mater. Res. Bull. 3 (1968) 37–46, https://doi.org/10.1016/0025-5408(68)90023-8.

[43] G. Senthil Murugan, Y. Ohishi, $TeO_2–BaO–SrO–Nb_2O_5$ glasses: a new glass system for waveguide devices applications, J. Non Cryst. Solids 341 (2004) 86–92, https://doi.org/10.1016/j.jnoncrysol.2004.04.006.

[44] F. Urbach, The long-wavelength edge of photographic sensitivity and of the electronic absorption of solids, Phys. Rev. 92 (1953) 1324 https://doi.org/10.1103/PhysRev.92.1324, 1324.

[45] S. Rani, S. Sanghi, A. Agarwal, S. Khasa, Influence of Nb_2O_5 on the optical band gap and electrical conductivity of Nb_2O_5-BaO-B_2O_3, IOP Conf. Ser. Mater. Sci. Eng. 2 (2009) 012041, https://doi.org/10.1088/1757-899X/2/1/012041.

[46] J.A. Duffy, M.D. Ingram, An interpretation of glass chemistry in terms of the optical basicity concept, J. Non Cryst. Solids 21 (1976) 373–410, https://doi.org/10.1016/0022-3093(76)90027-2.

[47] T. Honma, Y. Benino, T. Fujiwara, T. Komatsu, R. Sato, V. Dimitrov, Electronic polarizability, optical basicity, and interaction parameter of La_2O_3 and related glasses, J. Appl. Phys. 91 (2002) 2942–2950, https://doi.org/10.1063/1.1436292.

[48] J.A. Duffy, Trends in energy gaps of binary compounds: an approach based upon electron transfer parameters from optical spectroscopy, J. Phys. C Solid State Phys. 13 (1980) 2979–2989, https://doi.org/10.1088/0022-3719/13/16/008.
[49] K. Binnemans, Interpretation of Europium(III) spectra, Coord. Chem. Rev. 295 (2015) 1–45, https://doi.org/10.1016/j.ccr.2015.02.015.
[50] A.L. Pena, J.M.M. Buarque, M.A. Schiavon, J.L. Rangel, I. Carvalho, R.R. Gonçalves, J.L. Ferrari, Structural and optical investigations of Eu^{3+} -doped TiO_2 nanopowders, Ceram. Int. 42 (2016) 6914–6923, https://doi.org/10.1016/j.ceramint.2016.01.077.
[51] B. Milićević, V. Đorđević, K. Vuković, G. Dražić, M.D. Dramićanin, Effects of Li + co-doping on properties of Eu^{3+} activated TiO_2 anatase nanoparticles, Opt. Mater. 72 (2017) 316–322 https://doi.org/10.1016/j.optmat.2017.06.029 (Amst).
[52] C. Tregidgo, J.A. Levitt, K. Suhling, Effect of refractive index on the fluorescence lifetime of green fluorescent protein, J. Biomed. Opt. 13 (2008) 031218, https://doi.org/10.1117/1.2937212.
[53] M.R. Dousti, G.Y. Poirier, A.S.S. de Camargo, Structural and spectroscopic characteristics of Eu^{3+}-doped tungsten phosphate glasses, Opt. Mater. 45 (2015) 185–190 https://doi.org/10.1016/j.optmat.2015.03.033 (Amst).
[54] H. Huang, G.Q. Xu, W.S. Chin, L.M. Gan, C.H. Chew, Synthesis and characterization of Eu:Y_2O_3 nanoparticles, Nanotechnology 13 (2002) 318, https://doi.org/10.1088/0957-4484/13/3/316.
[55] L.L. Santos Alves, R.C. de Lima, M.A. Schiavon, R.R. Gonçalves, H.P. Barbosa, J.L. Ferrari, Photoluminescence properties of the material based on SiO_2–Y_2O_3:eu^{3+},Tb^{3+} under different *in situ* temperature prepared by the sol-gel process, J. Lumin. 222 (2020) 117109, https://doi.org/10.1016/j.jlumin.2020.117109.
[56] J.M.M.M. Buarque, D. Manzani, S.L. Scarpari, M. Nalin, S.J.L.L. Ribeiro, J. Esbenshade, M.A. Schiavon, J.L. Ferrari, SiO_2-TiO_2 doped with Er^{3+}/Yb^{3+}/Eu^{3+} photoluminescent material: a spectroscopy and structural study about potential application for improvement of the efficiency on solar cells, Mater. Res. Bull. 107 (2018) 295–307, https://doi.org/10.1016/j.materresbull.2018.07.007.
[57] R.V. Perrella, I.C. Ribeiro, P.H.A. Campos-Junior, M.A. Schiavon, E. Pecoraro, S.J.L. Ribeiro, J.L. Ferrari, $CaTiO_3$:Er^{3+}:Yb^{3+} upconversion from 980 nm to 1550 nm excitation and its potential as cells luminescent probes, Mater. Chem. Phys. 223 (2019) 391–397, https://doi.org/10.1016/j.matchemphys.2018.11.018.
[58] F. Auzel, Upconversion and anti-stokes processes with f and d ions in solids, Chem. Rev. 104 (2004) 139–174, https://doi.org/10.1021/cr020357g.
[59] F. Auzel, Upconversion processes in coupled ion systems, J. Lumin. 45 (1990) 341–345, https://doi.org/10.1016/0022-2313(90)90189-I.
[60] T.B. Paolini, SpectraChroma, (2021) 1–1. 10.5281/zenodo.4906590.
[61] F.T. Aquino, R.R. Pereira, J.L. Ferrari, S.J.L. Ribeiro, A. Ferrier, P. Goldner, R.R. Gonçalves, Unusual broadening of the NIR luminescence of Er^{3+}-doped Nb_2O_5 nanocrystals embedded in silica host: preparation and their structural and spectroscopic study for photonics applications, Mater. Chem. Phys. 147 (2014), https://doi.org/10.1016/j.matchemphys.2014.06.016.
[62] D.H.S. Reis, E. Pecoraro, F.C. Cassanjes, G.Y. Poirier, R.R. Gonçalves, J. Esbenshade, S.J.L. Ribeiro, M.A. Schiavon, J.L. Ferrari, Multifunctional possible application of the Er^{3+}/Yb^{3+}-coped Al_2O_3 prepared by recyclable precursor (aluminum can) and also by sol-gel process, Opt. Mater. 84 (2018) 504–513 https://doi.org/10.1016/j.optmat.2018.07.017 (Amst).